VIRAL IMMUNOLOGY
Volume 00, Number 00, 2020

Pp. 1–9
DOI: 10.1089/vim.2020.0018

Cryo-Electron Microscopy Structures of the *Pneumoviridae* Polymerases

Dongdong Cao and Bo Liang

Abstract

The resolution revolution of cryo-electron microscopy (cryo-EM) has made a significant impact on the structural analysis of the *Pneumoviridae* multifunctional RNA polymerases. In recent months, several high-resolution structures of *apo* RNA polymerases of *Pneumoviridae*, which includes the human respiratory syncytial virus (HRSV) and human metapneumovirus (HMPV), have been determined by single-particle cryo-EM. These structures illustrated high similarities and minor differences between the *Pneumoviridae* polymerases and revealed the potential mechanisms of the *Pneumoviridae* RNA synthesis.

Keywords: cryo-EM, structure, *Pneumoviridae*, polymerases, human respiratory syncytial virus, human metapneumovirus

Introduction

Resolution revolution of cryo-electron microscopy

Cryo-electron microscopy (cryo-EM) is an imaging technique for biological samples that are flash-frozen in the native environment as vitreous ice at cryogenic temperature (100 K). With recent breakthroughs of detector technology and image processing algorithms, cryo-EM leads to the resolution revolution and becomes a primary tool for the determination of macromolecular structures at near-atomic resolution, in addition to X-ray crystallography and nuclear magnetic resonance, without the need of crystals (8,38,43). The revolution is still ongoing, with increasing numbers of macromolecular assemblies being determined in different conformational states, higher resolutions being achieved, and symmetry limits being overcome (41). Collectively, cryo-EM is well suited for large heterogeneous assemblies and systems traditionally challenging for structural characterization (7,14,39).

One such challenging system is the RNA polymerase of the order of *Mononegavirales*, known as nonsegmented negative sense RNA viruses, which includes many significant human pathogens such as rabies virus, Ebola virus, and human respiratory syncytial virus (HRSV). There are currently eight virus families in the order of *Mononegavirales*, and *Pneumoviridae* is a new virus family since 2016 (used to be a subfamily *Pneumovirinae* in *Paramyxoviridae*) (2,30). *Pneumoviridae* has two genera, *Orthopneumovirus* and *Metapneumovirus*, with HRSV and human metapneumovirus (HMPV), the extensively studied representative, respectively. Both HRSV and HMPV cause severe respiratory diseases in young children, older adults, and immunocompromised patients worldwide (28,42,44). Currently, there is no effective vaccine nor antiviral therapy available to prevent or treat HRSV or HMPV infections (12,13,18,40). There are many unique aspects of RNA synthesis by the *Pneumoviridae* polymerases that make the polymerases attractive antiviral drug targets. Therefore, understanding the mechanisms of how *Pneumoviridae* polymerases function is a critical need for antiviral drug development.

RNA synthesis of Pneumoviridae

The RNA polymerase of *Pneumoviridae*, including that of HRSV and HMPV, is a large multifunctional polymerase complex that catalyzes three distinct enzymatic activities, namely, RNA dependent RNA polymerase (RdRp), capping (Cap), and cap methyltransferase (MT). The *Pneumoviridae* RNA polymerase is composed of two proteins, a large protein (L) and a tetrameric phosphoprotein (P). The *Pneumoviridae* L protein is a single polypeptide that contains all three catalytic domains that are necessary for RNA synthesis, cap addition, and cap methylation. The *Pneumoviridae* P protein is a tetramer in solution and the cofactor that regulates the activities of the L protein.

Pneumoviridae shares a common strategy of viral RNA synthesis (9,45), and it is believed to follow the ''start-stop

Department of Biochemistry, Emory University School of Medicine, Atlanta, Georgia, USA.

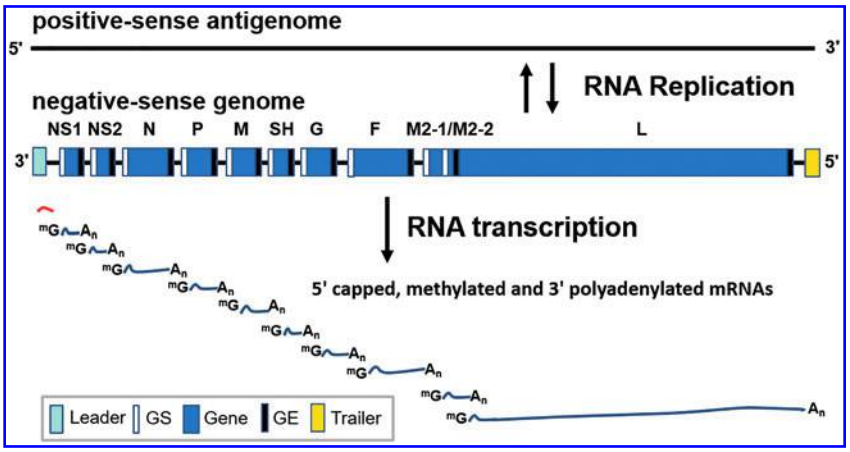

FIG. 1. The genome organization and RNA synthesis of the *Pneumoviridae* family. The negative-sense RSV genome is depicted 3′- > 5′ showing the leader (Le), trailer (Tr), GS, and GE regions that contain essential *cis-acting* signals for RNA synthesis. In *Pneumoviridae*, at each GS and GE, the highly conserved sequence provides critical signals for initiation and capping of downstream mRNAs and termination and polyadenylation of upstream mRNAs, respectively. The viral protein genes are shown above the mRNAs that are sequentially transcribed from them. Noncapped leader transcripts are colored in *red*. GE, gene end; GS, gene start; mRNAs, messenger RNAs.

model'' of sequential transcription (1,3) (features highlighted in Fig. 1). According to the ''start-stop model,'' (i) the polymerase recognizes a single promoter element of the leader region (3′ end of the negative-sense RNA genome) to start RNA synthesis; and (ii) the polymerase begins to synthesize messenger RNA (mRNA) in response to the first gene-start (GS) sequence (26). Immediately following transcription initiation, L caps the nascent mRNA by recognizing a specific *cis-acting* element at its 5′ end. The cap structure is further modified by L to become methylated at guanine-N-7 (N-7) and ribose 2′-hydroxyl (2′-O) positions. A *cis-acting* sequence gene end (GE) signals polyadenylation and termination; (iii) the polymerase stays on the template, reinitiates and caps the downstream mRNAs, and terminates and polyadenylates the upstream mRNAs in response to GS and GE signals of downstream genes (26,27); (iv) Like other *Mononegavirales*, the attenuation of the downstream mRNA occurs at each gene junction for most genes (25). Recent studies indicated the existence of nongradient and genotype-dependent transcription in RSV, suggesting the possibility of such nongradient gene expression in other *Mononegavirales* (34,36). Through this process of sequential attenuation of transcription, L produces ten viral mRNAs with appropriate ratios (32) (Fig. 1). Besides ''start-stop'' sequential transcription, L produces a leader (Le) RNA that remains uncapped and nonpolyadenylated when L initiates at the 3' end of the genomic RNA (9,33,45). For replication, L initiates at the 3' end of the Le or trailer complementary (TrC) sequences. However, during replication, L ignores all *cis-acting* regulatory signals to produce a full-length uncapped antigenome RNA instead (16). Unlike transcription, RNA replication is dependent upon ongoing protein synthesis to supply N protein to encapsidate the newly synthesized RNA (17).

Multiple cryo-EM structures of the Pneumoviridae *polymerases*

Due to the relatively large size of L (more than 2,000 residues in length and ~250 kDa in molecular weight) with multiple domains and a tetrameric P that is intrinsically flexible, it is challenging to obtain crystals of the *Pneumoviridae* polymerase complexes for X-ray crystallography. As mentioned above, cryo-EM offers an alternative method for high-resolution structural characterization of such macromolecular complexes with limited sample quantity requirements. In recent months, there have been multiple successful reports of the structural characterizations of the *Pneumoviridae* polymerases by cryo-EM, two of which for HRSV (PDB: 6PZK, EMDB: EMD-20536 & PDB: 6UEN, EMDB: EMD-20754) and one for HMPV (PDB: 6U5O, EMDB: EMD-20651) (6,19,35).

The structures of the *Pneumoviridae* polymerases provide enriched insights into how the *Pneumoviridae* polymerases function. The 3.2 Å (PDB: 6PZK) and 3.67 Å (PDB: 6UEN) resolution structures of the HRSV polymerase complexes share an overall nearly identical architecture (root-mean-square deviation [RMSD] between 6PZK and 6UEN is about 1 Å) (6,19) (Fig. 2). The linear domain representation and structural organization are colored by domains (Fig. 2A). The representative raw cryo-EM micrograph, two-dimension class averages, and the three-dimension (3D) reconstruction of the HRSV polymerase (EMD-20754) are shown in Figure 2B–D. Both structures reveal that the RNA dependent RNA polymerase (RdRp, blue) and capping (Cap, green) domains of L bound with the oligomerization domain (P_{OD}, red) and C-terminal domain (P_{CTD}, orange) of a tetramer of P. Interestingly, although both studies used full-length L and P proteins, the electron densities of MT domain and structural domains (connector domain [CD] and C-terminal domain [CTD]) of the HRSV L and the N-terminal domain of the HRSV P (P_{NTD}) are missing in both 3D reconstructions (6,19) (Fig. 2E, missing domains are shown in gray in Fig. 2A). The integrity of the proteins was validated by mass spectrometry, and the missing electron densities suggest that those domains are disordered (6). Those disordered domains are likely intrinsically flexible, and the binding of the P tetramer to L is not sufficient to lock those domains into a stable conformation. Further

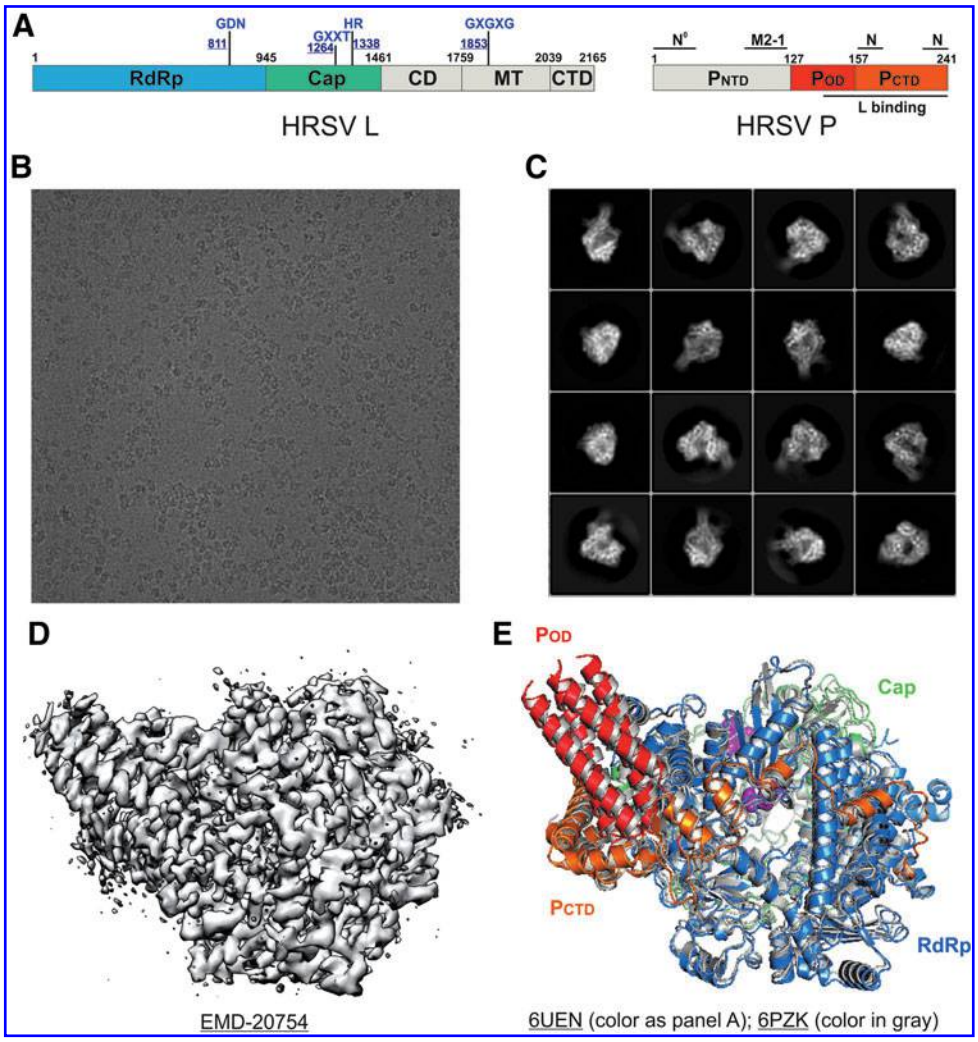

FIG. 2. The cryo-EM structures of the HRSV polymerases. **(A)** Linear domain representation with the boundary of the L and P proteins of the HRSV. The RdRp domain and Cap domain of L, as well as the oligomerization domain (P_{OD}) and C-terminal domain (P_{CTD}) of a tetramer of P, are colored in *blue*, *green*, *red*, and *orange*, respectively. The key residues for each functional domain are highlighted above with residue numbers. The unobserved domains are colored in *gray*. The representative raw cryo-EM micrograph **(B)**, 2D class averages **(C)**, and the 3D reconstruction **(D)** of the HRSV polymerase (EMDB: EMD-20754). **(E)** The structural comparison between 3.67 Å (PDB: 6UEN, colored as **A)** and 3.2 Å (PDB: 6PZK, colored in *gray*) structures of the HRSV polymerase complexes. The PDB and EMDB accession codes are *underlined*. 2D, two-dimension; 3D, three-dimension; Cap, capping; Cryo-EM, cryo-electron microscopy; HRSV, human respiratory syncytial virus; RdRp, RNA dependent RNA polymerase.

comparison of both structures reveals almost identical individual domains but slightly different intermolecular arrangements, suggesting the plasticity of the L:P interface, which may adopt a more substantial rearrangement during RNA synthesis (6).

Remarkably, the 3.7 Å resolution structure of the HMPV polymerase (PDB: 6U5O) shared a highly similar architecture to that of the HRSV polymerase that the RdRp and Cap domains of the HMPV L bind with a tetramer of the HMPV P (32). The linear domain representation and the boundaries of the HMPV L and P are shown in Figure 3A. The RMSD between HRSV and HMPV polymerase is less than 1.5 Å. Similarly, the MT and other structural domains (CD and CTD) of L and P_{NTD} are also missing in the structure of the HMPV polymerase complex (Fig. 3B). The identities of both full-length HMPV L and P proteins used for structural characterization were also confirmed by mass spectrometry (35). Similarly, those missing domains are likely to be disordered in solution.

The cryo-EM structure of a homologous Rhabdoviridae *polymerase*

The structure of L in complex with the N-terminal domain of P (P_{NTD}) of vesicular stomatitis virus (VSV), a member of the *Rhabdoviridae* family in the order of *Mononegavirales*, was determined by cryo-EM at 3.8 Å resolution (PDB: 5A22, EMDB: EMD-6337) in 2015 (29). This was the first structure of *Mononegavirales* polymerase, requiring *de novo* model building of the entire L protein. Except for a few flexible loops, all three functional domains,

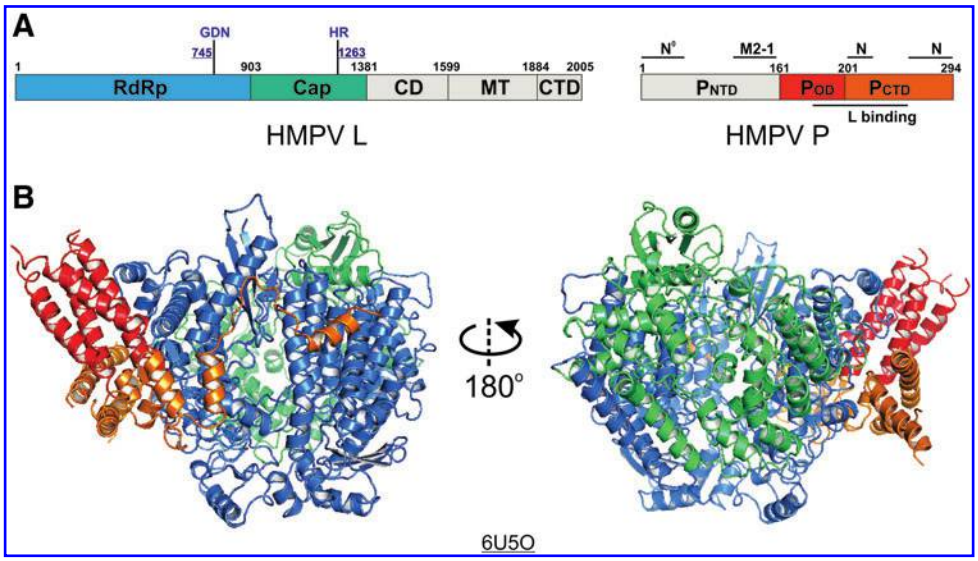

FIG. 3. The cryo-EM structure of the HMPV polymerase. **(A)** Linear domain representation with the boundary of the L and P proteins of the HMPV. The RdRp domain and Cap domain of L, as well as the oligomerization domain (P_{OD}) and C-terminal domain (P_{CTD}) of a tetramer of P, are colored in *blue*, *green*, *red*, and *orange*, respectively. The key residues for each functional domain are highlighted above with residue numbers. The missing domains are colored in *gray*. Note that the interaction domains of P with M2-1 and N have not been shown by experimental approaches but are speculative by analogy to RSV. **(B)** The 3.67 Å structure of the HMPV polymerase (PDB: 6U5O, colored as **A**). The PDB accession code is *underlined*. HMPV, human metapneumovirus.

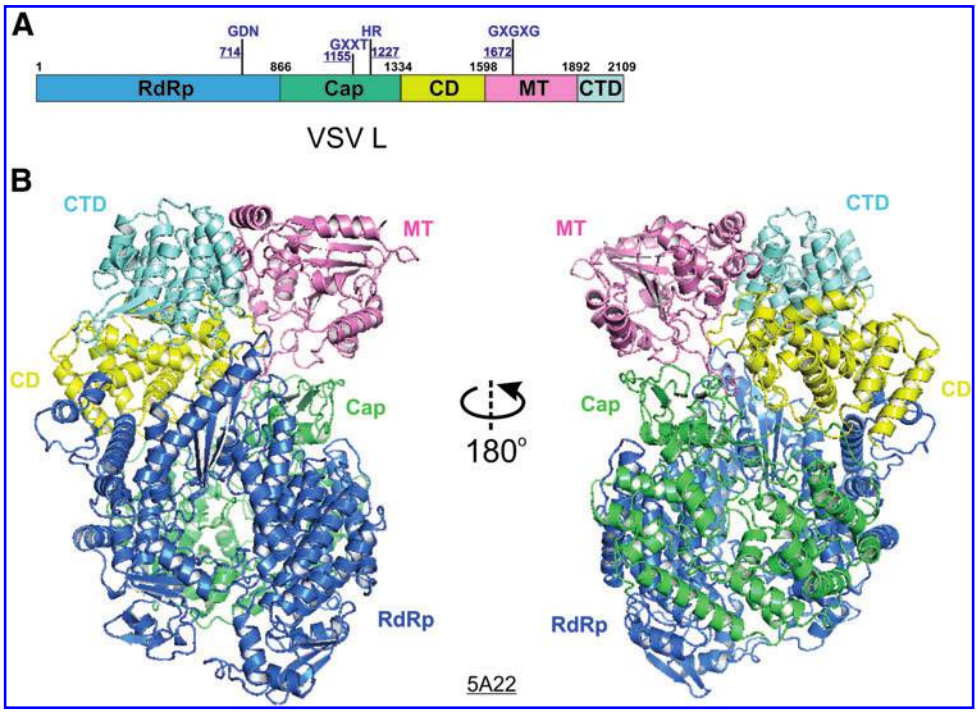

FIG. 4. The cryo-EM structure of the VSV L. **(A)** Linear domain representation with the boundary of the L protein of the VSV. The RdRp domain, Cap domain, CD, MT domain, and CTD of L are colored in *blue*, *green*, *yellow*, *pink*, and *cyan*, respectively. The key residues for each functional domain are highlighted above with residue numbers. **(B)** The 3.8 Å cryo-EM structure of the VSV L protein (PDB: 5A22) is colored as **(A)**. The PDB accession code is *underlined*. CD, connector domain; CTD, C-terminal domain; MT, methyltransferase; VSV, vesicular stomatitis virus.

the RdRp (blue), Cap (green), and MT (pink) domains, and two structural domains, the CD (yellow) and CTD (cyan), were resolved in the structure of the VSV L (Fig. 4). The linear domain organization is shown in Figure 4A. The RdRp domain resembles a right-hand thumb-palm-finger ring-like core domain configuration of DNA and RNA polymerases. The Cap domain of L folds next to the RdRp domain, and there was no available structural homology for the Cap domain due to the unconventional capping mechanism for *Mononegavirales*. Interestingly, there is a priming loop-like element in the Cap domain of the VSV L that is located next to the active site of the RdRp domain, which is speculated to function as a priming loop responsible for the *de novo* initiation of the RNA synthesis. The MT domain is separated from the Cap domain by the CD domain and then followed by the CTD (Fig. 4B). Due to the compact packing of the RdRp and Cap domains, the position of the priming loop-like element, and no distinct RNA product exit channel, it is speculated that the L adopts a preinitiation state, and significant rearrangements of those domains are likely to occur during other states of RNA synthesis.

Structural comparison of the Pneumoviridae *polymerases*

Recently, two high-resolution structures of the polymerases (L:P complexes) of *Rhabdoviridae* were reported (22,23). Given the relative conservation between the L proteins of *Pneumoviridae* and *Rhabdoviridae* (17–19% sequence identity), it was initially thought that the

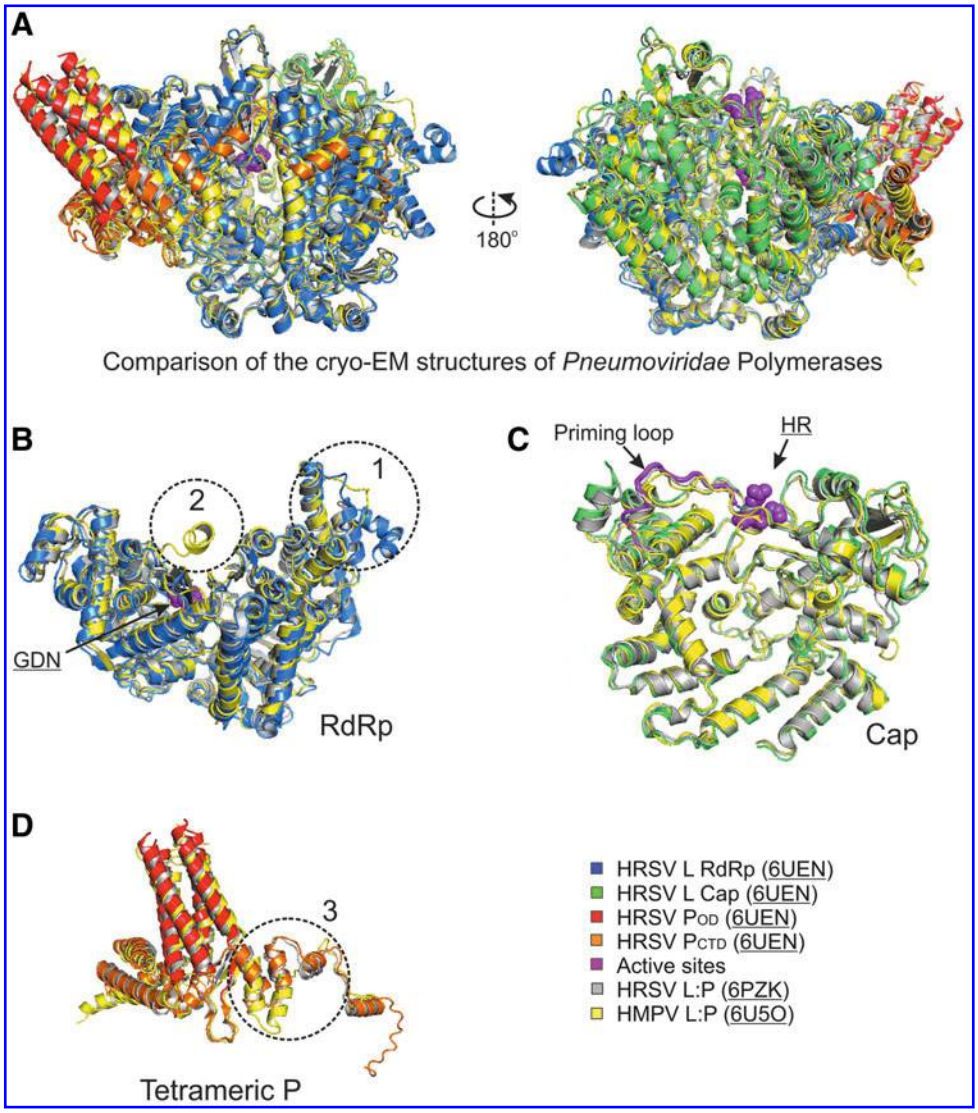

FIG. 5. Structural comparison of the *Pneumoviridae* polymerases. **(A)** The structural comparison of the 3.67 Å (PDB: 6UEN, colored as Fig. 2) and 3.2 Å (PDB: 6PZK, *gray*) structures of the HRSV polymerase complexes, as well as 3.7 Å (PDB: 6U5O, *yellow*) structure of the HMPV polymerase complex. **(B)** The RdRp domain of the L protein with the active sites GDN highlighted in *magenta*. **(C)** The Cap domain of the L protein with the active sites HR and priming loop highlighted in *magenta*. **(D)** The P_{OD} and P_{CTD} of the tetrameric P are shown. The noticeable differences between the structures of HRSV and HMPV polymerases are *circled* and labeled 1–3. The PDB accession codes are *underlined*.

Pneumoviridae L might share similar overall architecture to the *Rhabdoviridae* L. Surprisingly, (i) only the RdRp and Cap domains of the *Pneumoviridae* L are visible, although both domains display similar folds to that of the *Rhabdoviridae* L; (ii) the priming loop-like element of the Cap domain of *Pneumoviridae* shows a significant shift compared to its equivalent motif of the *Rhabdoviridae* L, suggesting that the *Pneumoviridae* L is in an elongation-compatible state (Fig. 5C). Furthermore, the interactions between P and L are shown differently in *Pneumoviridae* and *Rhabdoviridae*, which may be mainly due to different domains of P that are visible in the structures, the P_{OD} and P_{CTD} in *Pneumoviridae* and the P_{NTD} in *Rhabdoviridae*, respectively (6,19,22,23,35). In general, the structures of the HRSV and HMPV polymerases share similar active sites GDN and HR for RdRp and Cap domains, respectively (Fig. 5B, C, highlighted in magenta spheres, Fig. 6A, highlighted in magenta text).

Further comparison of the cryo-EM structures of HRSV and HMPV polymerases reveals that (i) the region (residues 134–176, HRSV L) in the RdRp of HRSV is mostly flexible, and some parts are not traceable, but the same region of HMPV has much shorter sequences and it is ordered (Fig. 5B, circle 1, sequence alignment in Fig. 6A), (ii) the RdRp of HRSV has a missing connecting helix (residues 660–691, HRSV L; equivalent to residues 571–597, VSV L) adjacent to the active site, providing sufficient space to accommodate RNA during RNA synthesis; however, this connecting helix can be partially modeled in the RdRp of HMPV (Fig. 5B, circle 2), (iii) the Cap domain of the HRSV L is similar to that of the HMPV L, including the priming loop-like element (magenta tubes) (Fig. 5C), and (iv) one chain of the HRSV P tetramers shows a different arrangement concerning that of the HMPV P (Fig. 5D, circle 3, sequence alignment in Fig. 6B). Those highlighted regions show subtle differences between two subfamilies, and those regions most likely contribute to the subfamily specific interactions within the RNA synthesis machine or with the host factors.

Summary

Undoubtedly, with the resolution revolution and small sample quantity requirement, cryo-EM offers an attractive solution to characterize the structural basis of challenging biological systems, such as the multifunctional *Pneumoviridae* polymerases. As a result, three high-resolution cryo-EM structures of the *Pneumoviridae* polymerases have been determined within the last few months (6,19,35). Such fast advancements reflect the power of cryo-EM as a tool for structural analysis of the *Pneumoviridae* polymerase complexes at different stages going forward.

As a multifunctional enzyme, the counterparts of the RdRp domain of L in eukaryotic cells are RNA polymerase (such as RNA polymerase II) (11,20), and the counterparts of the Cap and MT domains of L are RNA triphosphatase, guanylyltransferase, and MT, three of which are responsible for the addition of the methylated 5′ cap to the mRNA (10,15,21,24,31,37). Besides, L also polyadenylates at the 3′ end of the nascent mRNA, where the same process needs multiple enzymes to first cleave the 3′ end by a set of proteins (such as CPSF, CstF, and CFI) and then add the poly(A) tail by a polyadenylate polymerase (4,5,10,15,21,24,31,37). Remarkably, the same L protein ignores all transcriptional signals to replicate the entire genome during replication, without capping and polyadenylation. Therefore, it is intriguing to know how the polymerase interacts with RNA and how drugs would inhibit the functions of the polymerase. So far, there are no structures of *Pneumoviridae* polymerases in complex of RNA or inhibitors, and the modeling of the potential RNA interactions and druggable sites are described (6).

In summary, the sequence identities of L and P proteins between HRSV and HMPV are 48% and 36%, respectively (Fig. 6). As expected, the high structural similarity of the *Pneumoviridae* polymerases agrees with the high sequence conservation. Nonetheless, the structural differences also reflect the missing or insertion regions compared to each other. Collectively, those high-resolution cryo-EM structures provide insights into the molecular architectures, the interaction surfaces, the RNA synthesis mechanism, and the inhibitor developments of the *Pneumoviridae* polymerases.

Acknowledgments

The authors thank the members of the Liang lab for helpful support.

Author Disclosure Statement

The authors declare no competing interests.

Funding Information

The research programs in the B.L. laboratory are supported by the US National Institute of General Medical Sciences (NIGMS), National Institutes of Health (NIH)

FIG. 6. Sequence alignment of the *Pneumoviridae* L and P. The sequence alignment of the L proteins **(A)** and the P proteins **(B)** from HRSV strain A2 (Uniprot: P28887 for L and P03421 for P), bovine respiratory syncytial virus strain A51908 (Uniprot: O91940 for L and P33454 for P), murine pneumonia virus strain 15 (Uniprot: Q50EW2 for L and Q5MKM7 for P), avian metapneumovirus isolate Canada goose/Minnesota/15a/2001 (Uniprot: Q2Y2L8 for L and Q2Y2M5 for P), and HMPV strain CAN97-83 (Uniprot: Q6WB93 for L and Q8B9Q8 for P). The sequence identities of the L protein of BRSV, HMPV, AMPV, and MPV compared to HRSV are 84.17%, 47.97%, 48.08%, and 53.49%, respectively. The sequence identities of the P protein of BRSV, HMPV, AMPV, and MPV compared to HRSV are 81.25%, 34.36%, 35.68%, and 39.91%, respectively. The domains that are visible in the structures are *boxed* using the same *color* as Figures 2 and 3. The active sites GDN of the RdRp domain and HR of the Cap domain are highlighted in *magenta*. The alignments are prepared with Multalin and ESPript.

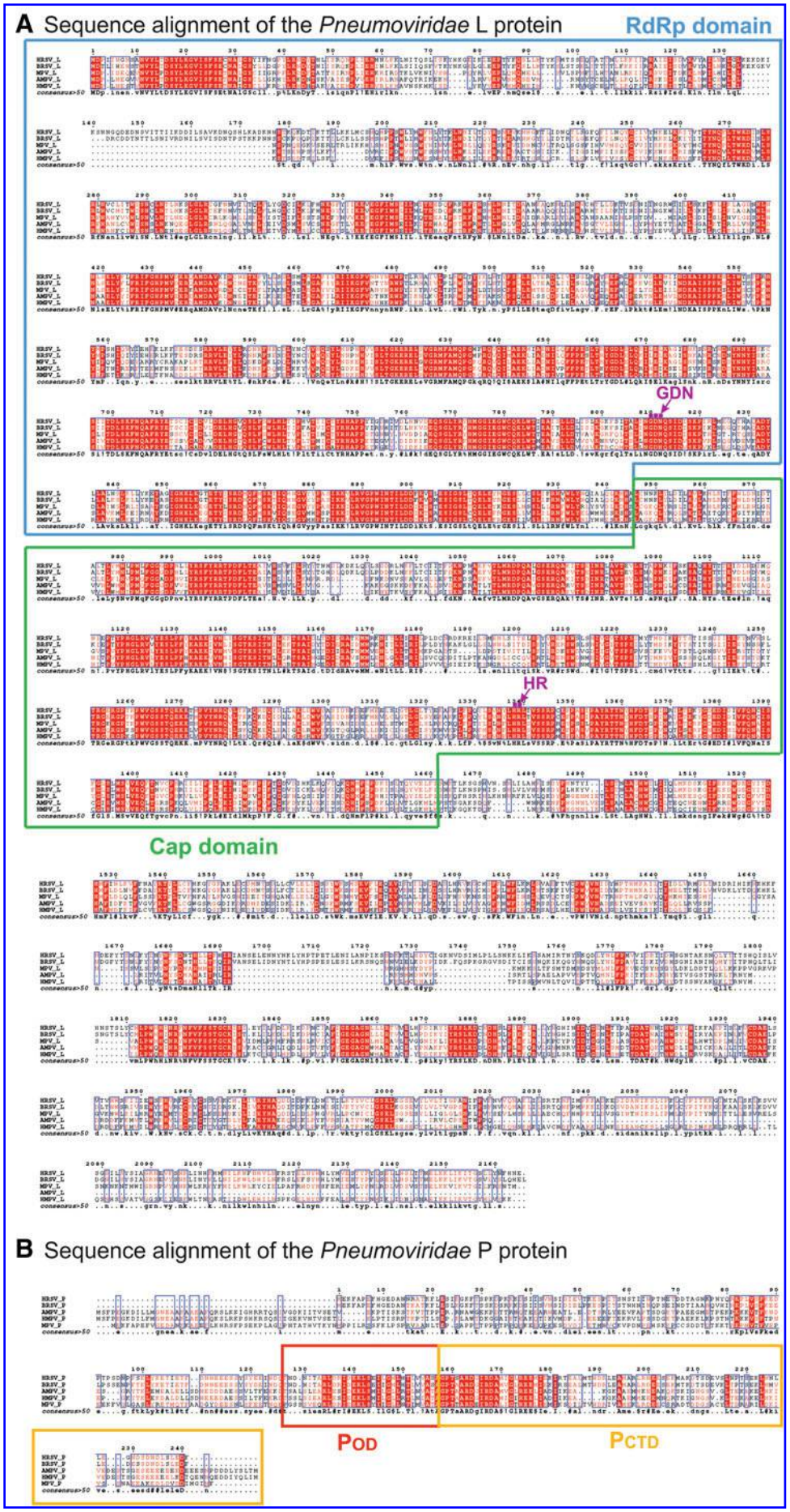

under award number R01GM130950, and the Research Start-Up Fund at Emory University School of Medicine.

References

1. Abraham G, and Banerjee AK. Sequential transcription of the genes of vesicular stomatitis virus. Proc Natl Acad Sci U S A 1976;73:1504–1508.
2. Afonso CL, Amarasinghe GK, Bányai K, *et al.* Taxonomy of the order Mononegavirales: update 2016. Arch Virol 2016;161:2351–2360.
3. Ball LA, and White CN. Order of transcription of genes of vesicular stomatitis virus. Proc Natl Acad Sci U S A 1976; 73:442–446.
4. Balbo PB, and Bohm A. Mechanism of poly(A) polymerase: structure of the enzyme-MgATP-RNA ternary complex and kinetic analysis. Structure 2007;15:1117–1131.
5. Bienroth S, Keller W, and Wahle E. Assembly of a processive messenger RNA polyadenylation complex. EMBO J 1993;12:585–594.
6. Cao D, Gao Y, Roesler C, *et al.* Cryo-EM structure of the respiratory syncytial virus RNA polymerase. Nat Commun 2020;11:368.
7. Cheng Y. Single-particle cryo-EM-How did it get here and where will it go. Science 2018;361:876–880.
8. Cheng Y, Glaeser RM, and Nogales E. How cryo-EM became so hot. Cell 2017;171:1229–1231.
9. Conzelmann KK. Nonsegmented negative-strand RNA viruses: genetics and manipulation of viral genomes. Annu Rev Genet 1998;32:123–162.
10. Cowling VH. Regulation of mRNA cap methylation. Biochem J 2009;425:295–302.
11. Cramer P, Bushnell DA, and Kornberg RD. Structural basis of transcription: RNA polymerase II at 2.8 angstrom resolution. Science 2001;292:1863–1876.
12. Cui R, Wang Y, Wang L, *et al.* Cyclopiazonic acid, an inhibitor of calcium-dependent ATPases with antiviral activity against human respiratory syncytial virus. Antiviral Res 2016;132:38–45.
13. Deffrasnes C, Hamelin ME, Prince GA, and Boivin G. Identification and evaluation of a highly effective fusion inhibitor for human metapneumovirus. Antimicrob Agents Chemother 2008;52:279–287.
14. Earl LA, Falconieri V, Milne JL, and Subramaniam S. Cryo-EM: beyond the microscope. Curr Opin Struct Biol 2017;46:71–78.
15. Fabrega C, Hausmann S, Shen V, Shuman S, and Lima CD. Structure and mechanism of mRNA cap (guanine-N7) methyltransferase. Mol Cell 2004;13:77–89.
16. Fearns R, Collins PL, and Peeples ME. Functional analysis of the genomic and antigenomic promoters of human respiratory syncytial virus. J Virol 2000;74:6006–6014.
17. Fearns R, Peeples ME, and Collins PL. Increased expression of the N protein of respiratory syncytial virus stimulates minigenome replication but does not alter the balance between the synthesis of mRNA and antigenome. Virology 1997;236:188–201.
18. Feuillet F, Lina B, Rosa-Calatrava M, and Boivin G. Ten years of human metapneumovirus research. J Clin Virol 2012;53:97–105.
19. Gilman MSA, Liu C, Fung A, *et al.* Structure of the respiratory syncytial virus polymerase complex. Cell 2019; 179:193.e14–204.e14.
20. Gnatt AL, Cramer P, Fu J, *et al.* Structural basis of transcription: an RNA polymerase II elongation complex at 3.3 A resolution. Science 2001;292:1876–1882.
21. Ho CK, Sriskanda V, McCracken S, *et al.* The guanylyltransferase domain of mammalian mRNA capping enzyme binds to the phosphorylated carboxyl-terminal domain of RNA polymerase II. J Biol Chem 1998;273: 9577–9585.
22. Horwitz JA, Jenni S, Harrison SC, and Whelan SPJ. Structure of a rabies virus polymerase complex from electron cryo-microscopy. Proc Natl Acad Sci U S A 2020; 117:2099–2107.
23. Jenni S, Bloyet LM, Diaz-Avalos R, *et al.* Structure of the vesicular stomatitis virus L protein in complex with its phosphoprotein cofactor. Cell Rep 2020;30:53.e5–60.e5.
24. Kim HJ, Jeong SH, Heo JH, *et al.* mRNA capping enzyme activity is coupled to an early transcription elongation. Mol Cell Biol 2004;24:6184–6193.
25. Kuo L, Fearns R, and Collins PL. The structurally diverse intergenic regions of respiratory syncytial virus do not modulate sequential transcription by a dicistronic minigenome. J Virol 1996;70:6143–6150.
26. Kuo L, Fearns R, and Collins PL. Analysis of the gene start and gene end signals of human respiratory syncytial virus: quasi-templated initiation at position 1 of the encoded mRNA. J Virol 1997;71:4944–4953.
27. Kuo L, Grosfeld H, Cristina J, *et al.* Effects of mutations in the gene-start and gene-end sequence motifs on transcription of monocistronic and dicistronic minigenomes of respiratory syncytial virus. J Virol 1996;70:6892–6901.
28. Li Y, Reeves RM, Wang X, *et al.* Global patterns in monthly activity of influenza virus, respiratory syncytial virus, parainfluenza virus, and metapneumovirus: a systematic analysis. Lancet Glob Health 2019;7:e1031–e1045.
29. Liang B, Li Z, Jenni S, *et al.* Structure of the L protein of vesicular stomatitis virus from electron cryomicroscopy. Cell 2015;162:314–327.
30. Maes P, Amarasinghe GK, Ayllón MA, *et al.* Taxonomy of the order Mononegavirales: second update 2018. Arch Virol 2019;164:1233–1244.
31. Mandal SS, Chu C, Wada T, *et al.* Functional interactions of RNA-capping enzyme with factors that positively and negatively regulate promoter escape by RNA polymerase II. Proc Natl Acad Sci U S A 2004;101: 7572–7577.
32. Mink MA, Stec DS, and Collins PL. Nucleotide sequences of the 3′ leader and 5′ trailer regions of human respiratory syncytial virus genomic RNA. Virology 1991;185:615–624.
33. Ogino T, and Green TJ. RNA Synthesis and capping by nonsegmented negative strand RNA viral polymerases: lessons from a prototypic virus. Front Microbiol 2019;10:1490.
34. Pagan I, Holmes EC, and Simon-Loriere E. Level of gene expression is a major determinant of protein evolution in the viral order Mononegavirales. J Virol 2012;86:5253–5263.

35. Pan J, Qian X, Lattmann S, *et al.* Structure of the human metapneumovirus polymerase phosphoprotein complex. Nature 2020;577:275–279.
36. Piedra FA, Qiu X, Teng MN, *et al.* Non-gradient and genotype-dependent patterns of RSV gene expression. PLoS One 2020;15:e0227558.
37. Proudfoot NJ, Furger A, and Dye MJ. Integrating mRNA processing with transcription. Cell 2002;108:501–512.
38. Raunser S. Cryo-EM revolutionizes the structure determination of biomolecules. Angew Chem Int Ed Engl 2017;56: 16450–16452.
39. Renaud JP, Chari A, Ciferri C, *et al.* Cryo-EM in drug discovery: achievements, limitations and prospects. Nat Rev Drug Discov 2018;17:471–492.
40. Rivera CA, Gómez RS, Díaz RA, *et al.* Novel therapies and vaccines against the human respiratory syncytial virus. Expert Opin Investig Drugs 2015;24:1613–1630.
41. Rivera-Calzada A, and Carroni M. Editorial: technical advances in Cryo-electron microscopy. Front Mol Biosci 2019;6:72.
42. Shah DP, Shah PK, Azzi JM, *et al.* Human metapneumovirus infections in hematopoietic cell transplant recipients and hematologic malignancy patients: a systematic review. Cancer Lett 2016;379:100–106.
43. Shen PS. The 2017 Nobel Prize in Chemistry: cryo-EM comes of age. Anal Bioanal Chem 2018;410:2053–2057.
44. Shi T, McAllister DA, O'Brien KL, *et al.* Global, regional, and national disease burden estimates of acute lower respiratory infections due to respiratory syncytial virus in young children in 2015: a systematic review and modelling study. Lancet 2017;390:946–958.
45. Whelan SP, Barr JN, and Wertz GW. Transcription and replication of nonsegmented negative-strand RNA viruses. Curr Top Microbiol Immunol 2004;283:61–119.

Address correspondence to:
Dr. Bo Liang
Department of Biochemistry
Emory University School of Medicine
Atlanta, GA 30322
USA

E-mail: bo.liang@emory.edu